

# Bayesian Algorithm Execution for Tuning Particle Accelerator Emittance with Partial Measurements

Sara Ayoub Miskovich<sup>1,\*</sup>, Willie Neiswanger<sup>2,†</sup>, William Colocho<sup>1</sup>, Claudio Emma<sup>1</sup>, Jacqueline Garrahan<sup>1</sup>, Timothy Maxwell<sup>1</sup>, Christopher Mayes<sup>1</sup>, Stefano Ermon<sup>2</sup>, Auralee Edelen<sup>1,‡</sup> and Daniel Ratner<sup>1,§</sup>

<sup>1</sup>SLAC National Laboratory, Menlo Park, California 94025, USA and

<sup>2</sup>Department of Computer Science, Stanford University, Stanford, California 94305, USA

(Dated: September 13, 2022)

Traditional black-box optimization methods are inefficient when dealing with *multi-point measurements*, i.e. when each query in the control domain requires a set of measurements in a secondary domain to calculate the objective. In particle accelerators, emittance tuning from quadrupole scans is an example of optimization with multi-point measurements. Although the emittance is a critical parameter for the performance of high-brightness machines, including X-ray lasers and linear colliders, comprehensive optimization is often limited by the time required for tuning. Here, we extend the recently-proposed Bayesian Algorithm Execution (BAX) to the task of optimization with multi-point measurements. BAX achieves sample-efficiency by selecting and modeling individual points in the joint control-measurement domain. We apply BAX to emittance minimization at the Linac Coherent Light Source (LCLS) and the Facility for Advanced Accelerator Experimental Tests II (FACET-II) particle accelerators. In an LCLS simulation environment, we show that BAX delivers a 20× increase in efficiency while also being more robust to noise compared to traditional optimization methods. Additionally, we ran BAX live at both LCLS and FACET-II, matching the hand-tuned emittance at FACET-II and achieving an optimal emittance that was 24% lower than that obtained by hand-tuning at LCLS. We anticipate that our approach can readily be adapted to other types of optimization problems involving multi-point measurements commonly found in scientific instruments.

## INTRODUCTION

Black-box optimization is a general approach for tuning tasks in which the system response is at least partially unknown [1, 2]. Examples of black-box optimizers include Nelder-Mead simplex, coordinate descent, genetic algorithms, and many others. Bayesian optimization (BO) [3, 4] is an especially appealing approach for black-box systems in which each function query is expensive (in time or other costs), a common situation for scientific and industrial instruments. BO has been used extensively for optimization of scientific instruments, including particle accelerators [5–9].

For applications where the optimization objective is not a direct system observable, but rather is computed from secondary measurements, even BO may be too inefficient. For example, a single query might require a scan of another variable, a complicated computation, or an internal optimization process. In this work we refer to this type of measurement as a *multi-point measurement*. Black-box optimization tasks with multi-point measurements are encountered in a variety of fields, such as bioinformatics [10], material science [11], and nuclear astrophysics [12], in addition to particle accelerators [13]. Traditional optimization methods, including BO, exhibit two types of inefficiencies on multi-point measurements.

First, each query requires a set number of secondary measurement points (i.e. *partial measurements*) even if a subset of those points already reveals the system settings to be sub-optimal. Second, because the black-box function returns only the objective to the optimization algorithm, the full information acquired within the black-box function evaluation (e.g. all partial measurements) is not shared across different optimization steps, and this information loss degrades the efficiency of the optimizer. The result is that each multi-point query is both *expensive and information-poor*. When time is a limiting factor, optimizer inefficiency may reduce the number of control variables that can be optimized, limit the ability to find a global optimum, or make the optimization task too costly to even attempt in practice. Optimizer inefficiency is particularly problematic for scientific instruments that are in high demand.

The motivating example for this paper is beam-emittance tuning in particle accelerators. The emittance of a charged particle beam, defined as the volume of particles in position-momentum phase space [14], is an important parameter for a variety of accelerator applications. For accelerator-based light sources, emittance determines the X-ray beam brightness, limiting the shortest wavelength available at X-ray free-electron lasers (XFELs) [15] and affecting the output X-ray power by orders of magnitude [16]. It is especially important for the next generation of undulator designs (e.g. LCLS-II-HE) [17]. For colliders, emittance tuning is critical to maximize luminosity [18, 19]. Beams optimized for high emittance ratios are needed for a variety of new light source and collider designs [20], and also for injection into components

\* smiskov@slac.stanford.edu; Shared co-first author.

† neiswanger@cs.stanford.edu; Shared co-first author.

‡ edelen@slac.stanford.edu

§ dratner@slac.stanford.edu

for compact accelerators, such as dielectric wakefield accelerating cavities [21].

Emittance depends on the initial beam conditions at the particle source (e.g. the photocathode and associated drive laser for electron accelerators), along with the combined effect of adjustable accelerator settings. The initial conditions can change as a result of both intended beam property adjustments (e.g. changes to the beam charge) and unintended drift over time (e.g. uncontrolled time-varying changes to the drive laser output). As a result, the accelerator settings need to be re-optimized, or *tuned*, to achieve acceptable emittance values periodically. Given the importance of the beam emittance to accelerator performance, emittance optimization would ideally be a routine task for accelerator operations.

However, one of the most common methods for determining the transverse emittance involves scanning a focusing magnet’s strength while observing the resulting change in beam size [14], i.e. the emittance is calculated from a multi-point measurement. Each step of the optimizer thus involves choosing a configuration in the control domain (the settings of accelerator), then taking a set of measurements over points in the secondary domain (in this case, beam-size measurements at different magnet settings), and finally fitting the points in the secondary domain to return an emittance value to the optimization algorithm. The inefficiency of measuring and in turn optimizing emittance severely limits the extent to which it is done in practice at most accelerator facilities, despite the importance of achieving small emittance. For example, at the Linac Coherent Light Source (LCLS) [15], injector emittance is typically tuned only after returning from a machine shut-down or a substantial change to the target beam parameters (such as the charge), and it is done almost entirely manually by human experts. There is a clear need for more efficient algorithms for emittance optimization.

We propose adapting a recently-developed method, Bayesian Algorithm Execution (BAX) [22], as a sample-efficient technique for optimization tasks with multi-point measurements. In contrast to BO, which directly models the objective function, BAX builds a model in the joint control-measurement domain, which is defined by the Cartesian product of the optimization’s control and secondary domains. As a result, BAX leverages all partial measurements, as opposed to modeling only the output of each multi-point query. In addition, by querying individual points in this joint control-measurement domain, BAX does not require a full multi-point measurement at each step. Modeling direct observables (e.g. beam sizes) rather than the objective (e.g. emittance) represents a conceptual shift in black-box optimization of multi-point measurements.

In summary, this paper extends the BAX algorithm to the challenging and outstanding problem of emittance tuning in accelerators, with substantial improvement in sample-efficiency. First, we describe how BAX can improve efficiency for general multi-point optimization

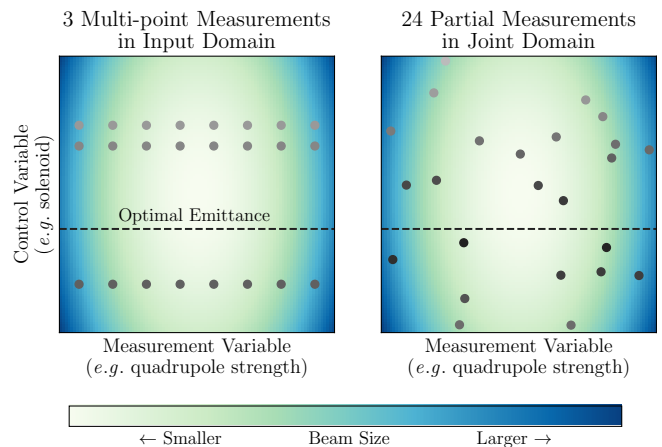


**FIG. 1: Querying the joint control-measurement domain.** Left: Illustration of multi-point measurements when tuning emittance with a standard black-box optimizer. The background color denotes the measured quantity (beam size), while the point color denotes the objective value (emittance) of the resulting multi-point query. The dashed line shows the optimal setting of the control variable. Optimizing the beam size is not equivalent to optimizing the emittance objective. Right: Illustration of the same number of beam-size measurements when optimizing via queries in the joint domain, maximizing information gain of each query.

tasks. Second, for the specific case of emittance optimization, we show BAX to be sample-efficient compared to both BO and the Nelder-Mead simplex algorithm [23], using a simulation environment of the LCLS injector. Finally, we show experimental results for BAX in minimization of electron beam emittance at both LCLS and the Facility for Advanced Accelerator Experimental Tests II (FACET-II) [24] at SLAC National Accelerator Laboratory (SLAC), with the former achieving 24% lower emittance than was found by manual tuning. We anticipate this approach to be widely adaptable to optimization problems involving multi-point measurements on real-world instruments in science and engineering.

## RESULTS

**Emittance measurement and optimization.** For illustration, a highly simplified layout of the LCLS injector and emittance measurement setup is shown in Fig. 3. A “quadrupole scan measurement” [14] of emittance works by scanning a quadrupole (denoted Q5) while measuring the beam size on a wire. Emittance can then be calculated from the parabolic behavior of beam size with respect to magnet settings. While single-shot emittance measurements for accelerators do exist (e.g. multi-slit and pepper-pot masks [25–28]), they are generally not suitable for all types of beams and beamline layouts, in-

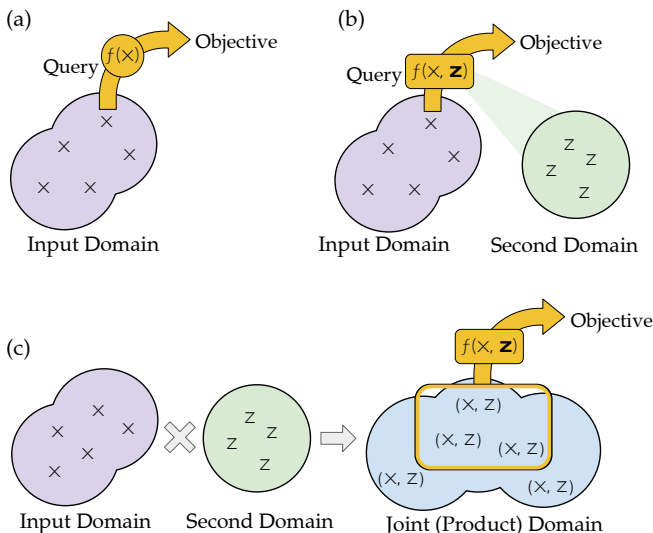


**FIG. 2: Direct optimization in the joint control-measurement domain.** (a) A simple query of some objective function  $f(x)$  is made at control setting  $x$  in the control domain. (b) A multi-point query at a control setting  $x$  requires a vector of measurements at a set of points  $z$  in a second domain. (c) The multi-point scenario is converted to an adaptive sampling problem in joint control-measurement domain.

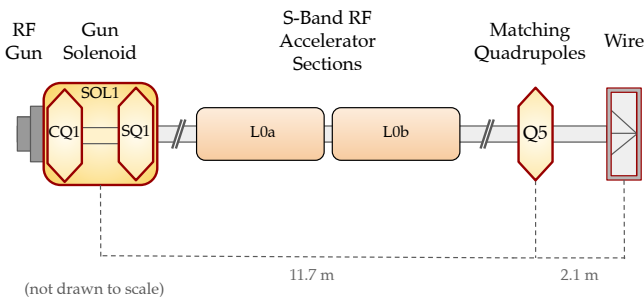


**FIG. 3: LCLS photoinjector layout.** The solenoid (SOL1) and corrector quadrupole (CQ1 and SQ1) settings comprise the control variables in our emittance optimization setting, and the quadrupole (Q5) setting is the measurement variable. The wire is used for beam-size measurements.

cluding beams at the LCLS.

Tuning accelerator parameters to minimize the emittance is a critical task at LCLS. The exact response of the emittance to accelerator settings is uncertain, and thus the emittance is typically tuned by iteratively adjusting settings and observing the outcome. Figure 3 shows three of the primary emittance-tuning variables: the solenoid magnet (SOL1) and two corrector quadrupoles (CQ1 and SQ1) [29]. Despite its importance, emittance tuning time is limited by the need to minimize beam interruptions to users, which roughly translates into a limit on the number

of queries to the system available for each tuning event.

With standard black-box emittance optimization, each step involves choosing a new control variable configuration (SOL1, CQ1, and SQ1 settings), running a sub-routine that measures the beam size at multiple settings of the magnet (Q5), and calculating the emittance from the set of beam sizes observed. At LCLS, the sub-routine is very time-consuming. When factoring in the need for robustness in automated tuning, we found that in practice we need to acquire an average of 18 beam-size measurements per emittance calculation, equivalent to 9 minutes of beam time per query. For additional details on the wire scanners, the emittance measurement, and the LCLS injector configuration, see the Methods section.

Figure 1 (a) highlights several problems encountered using BO—or other standard model-based optimizers—to tune emittance. As an illustration, we consider a typical emittance tuning task involving an eight-point measurement. First, BO must execute a full eight-measurement scan at each query, even if the first beam size indicates the control setting is poor. Second, despite the wealth of information in the beam-size measurements, BO only uses the calculated emittance to build its model. As a result, different steps of the optimizer acquire nearly redundant beam-size measurements. Third, the appropriate measurement variable settings depend on the control variables, which sometimes leads to scans that are unsuitable for fitting emittance and are discarded, despite being helpful for characterizing the beam-size response to the control variable. In standard optimization routines, this valuable information obtained during a failed scan would be discarded.

**BAX for efficient emittance optimization.** To improve the efficiency of a multi-point measurement optimization, we propose to model the joint control-measurement domain, e.g. to learn a model of beam size as a function of both control and measurement variables. Figure 1 (b) presents an illustration of how joint optimization increases the information gained from each individual beam-size measurement. In joint optimization, we require a method that minimizes a computed function (e.g. emittance) operating on a learned model of a direct observable (e.g. beam size). However, standard model-based optimization methods such as BO are restricted to modeling and optimizing the same quantity. In the case of emittance tuning, standard BO can only model and optimize the computed emittance from a full quadrupole scan at each query point in the control domain.

Instead of standard BO, we employ an information-based BAX method [22, 30, 31], which lets us model a direct observable and optimize the output of any function computed from that model, rather than the model itself. By employing BAX, we convert the joint optimization problem to a type of adaptive sampling (experimental design) [32, 33] problem in a joint control-measurement domain, as shown in Fig. 2. For each query from the control domain, instead of making a full measurement in the second domain, we evaluate a single point. In this

manner, each function query is cheap while still performing the same optimization problem, i.e. finding a point in the control domain that optimizes the black-box function. Full details on the BAX algorithm are described in the Methods section.

In the LCLS emittance application, BAX models the beam size with respect to the SOL1, CQ1, and SQ1 control variables and the Q5 quadrupole measurement variable. The full BAX emittance optimization procedure is illustrated in Fig. 4. The procedure is initialized with randomly sampled points from the joint control-measurement domain. Then, at each iteration, the BAX algorithm queries the beam-size measurement function at a single value of the Q5, SOL1, CQ1 and SQ1 variables, constructing a model of the beam size as a function of both control and measurement variables. This internal model represents the prior distribution on the function describing the beam-size response to the quadrupole strength, and is implemented in this work by a Gaussian process model (GP) with a radial basis function kernel.

During the internal step (Fig. 4b), BAX executes the emittance algorithm on a predefined number of quadrupole scans drawn from the model’s posterior distribution. Finally, the information-based BAX acquisition function selects a new beam-size measurement to query on the accelerator at the injector configuration that maximizes the information gain. Note that the query that maximizes the information gain is not necessarily the configuration with the lowest emittance based on the posterior samples. After measuring a new beam size, BAX updates the GP model and begins a new iteration. We emphasize that in a BAX emittance optimization, full emittance algorithm evaluations are only executed *on function samples drawn from the posterior distribution of the learned GP model, and never on the machine itself*.

In general, any automated emittance tuning approach requires a robust emittance calculation package. While BAX never executes a full emittance scan on the real machine, an equivalent method executes on the model posterior. In this paper we used the newly-developed `pyemittance` package [34] that provides adaptive emittance measurements. More details regarding the emittance measurement are described in the Methods section.

**Simulated Demonstration with Noisy Observations.** We study the performance of BAX in emittance optimization using a surrogate model of the LCLS copper injector trained on IMPACT-T simulation data. Details of this model are presented in the Methods section below. The BAX procedure queries the beam size from the LCLS surrogate model given a configuration of virtual injector control variables for SOL1, CQ1 and SQ1, as well as a single value for the Q5 strength. For each run, BAX was initialized with 10 points that were uniformly sampled from the joint control-measurement domain defined by the bounds set on each variable domain: SOL1: (0.46, 0.485) (kG·m), CQ1 and SQ1: (-0.02 0.02) (kG). All tests ran for 200 iterations, corresponding to 200 total

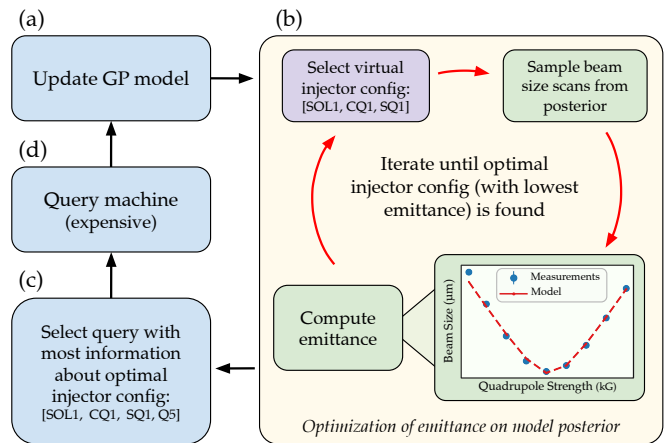


**FIG. 4: Diagram of the BAX procedure for emittance optimization.** (a) A GP models the beam-size function with respect to the three control variables (SOL1, CQ1, and SQ1) and measurement variable (Q5) based on experimental data. (b) BAX investigates the emittance value and uncertainty of different injector configurations (configs) with cheap queries of the GP posterior. (c) BAX suggests a new experimental data point based on the results of (b). (d) BAX queries the machine for a beam size. The colors of the boxes in this diagram match the colors of the domains illustrated in Fig. 2.

beam size queries from the simulation. Each algorithm execution on the posterior involves a scan of 10 initial points, followed by 10 final points in both  $X$  and  $Y$  after adjusting the scan range based on the minimum of the parabola (see Methods). To assess BAX’s performance, we repeat the optimization with black-box methods operating directly on the multi-point measurements. We chose Bayesian optimization (BO) and Nelder-Mead simplex [23] as baselines, as both have seen extensive use in accelerator operations [5–9, 35, 36]. Details of the BAX, BO, and simplex algorithm implementations are given in the Methods section.

For each algorithm, we ran 40 tests, each with different initial samples. For all simulation measurements, Gaussian noise of the form  $\mathcal{N}(0, \sigma_n)$  was added to the beam size for each function query, with  $\sigma_n = 10\%$  as a conservative estimate of typical experimental noise levels at LCLS (see Methods). Figure 5 shows the mean and standard error of the simulated BAX optimization runs (blue), Bayesian optimization with a GP model (orange), and simplex optimization runs (green). The emittance value shown is the ground truth (noiseless) emittance corresponding to the best control variables found at each iteration, and we display the best emittance up to that point as a function of the total number of beam-size measurements. The results are normalized by the ground truth optimal emittance. In the lower plot of Fig. 5, we show a magnified view of the BAX optimization. BAX never runs full emittance scans on the true function during optimization, so in practice an operator would not

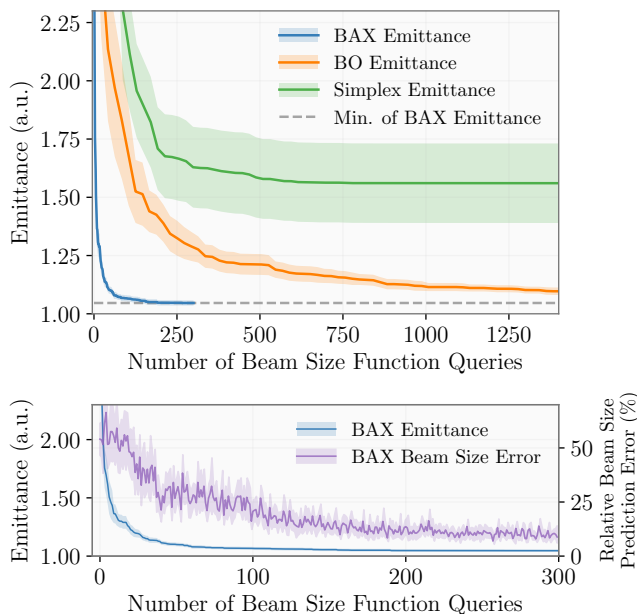


**FIG. 5: Simulated LCLS emittance optimization.**

Top: Optimization of beam emittance on the LCLS injector surrogate model using BAX (blue), BO (orange), and Nelder-Mead simplex optimization (green). The mean and 2-sigma standard error of 40 individual runs with randomized starting conditions are shown for each algorithm. The best emittance seen at each iteration is plotted, and the values are normalized by the minimum of the ground truth emittance. Bottom: A magnified view of BAX optimization results (blue), with the error on the BAX beam-size prediction compared to the true (observed) beam size in the LCLS surrogate model are shown on the right-hand axis (purple).

have access to the blue line. However, we can observe the quality of the internal beam-size model, which can serve as a proxy for convergence; if the BAX GP models the beam-size response correctly, it should also identify the configuration with the optimal emittance. For this reason, we also show the error on the BAX beam-size prediction compared to the true (observed) beam size in the LCLS surrogate model on the right-hand axis (purple).

We can further check that the BAX GP model learns the correct behavior of the beam size during scans over the secondary domain. Figure 6 shows samples of the GP posterior during iterations 40 and 100, with the control variables set to the optimal configuration that BAX estimates at that given iteration. By iteration 100, BAX models the beam-size response to a quadrupole scan with high accuracy.

It can be seen that BAX significantly surpasses BO and simplex in finding an optimal emittance by learning the behavior of the true beam size over the joint control-measurement domain in a sample-efficient manner. While each BO and simplex iteration corresponds to an average of 18 beam-size measurements, each BAX

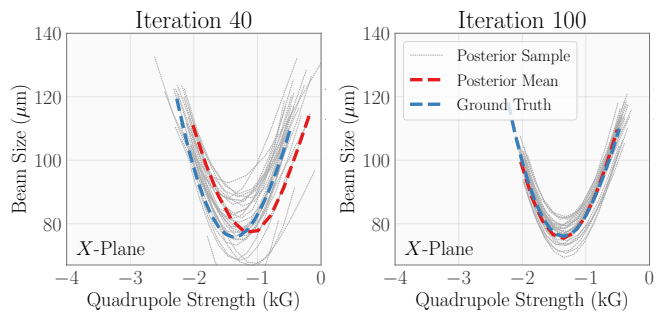


**FIG. 6: Posterior Samples in BAX.** Samples of the GP posterior during iterations 40 and 100 during a BAX optimization run on the LCLS surrogate model, with the control variables set to the optimal configuration that BAX estimates at the given iteration. We plot posterior samples of the emittance scan for these control variables (gray), the posterior mean of the GP at the same control variables (red), and the ground truth beam sizes for this scan (blue).

iteration is a single measurement. In this noisy environment, BAX finds the optimal emittance after about 160 measurements on average, while the mean of the BO runs takes over 3000. With each beam-size query taking 18 seconds on a wire scanner at LCLS, BAX would require 48 minutes of invasive beam-size measurements compared to 15 hours with BO.

We hypothesize that BAX should exhibit increased robustness to noise because its GP directly models the beam-size as opposed to the calculated emittance. To study BAX’s robustness to noise, we repeated the previous experiment with both a noisier (30%) and a less noisy (5%) beam-size function. The results are shown in Fig. 7: As we increase the noise added to the beam-size function, BAX’s performance is largely unchanged (blue), whereas BO’s performance is significantly hindered (orange).

**Experimental Demonstration.** We applied BAX to the online optimization of the beam emittance in the LCLS injector with an identical setup to the simulated environment. The injector control variables were the solenoid SOL1, and the two quadrupoles CQ1 and SQ1. The Q5 quadrupole was used for emittance measurements along with a downstream wire scanner. Details of the experimental setup is given in the Methods section. The bounds on the SOL1 device domain were identical to the simulation runs, (0.46, 0.485) (kG·m), while CQ1 and SQ1’s domains were made smaller to (-0.015, 0.015) (kG) due to constraints on the region where beam-size measurements were valid and within range of the wire scanner. In future work, such constraints can be incorporated in the optimization to learn to avoid bad or invalid regions without having to place tight restrictions on the control domains [37].

Figure 8 shows the resulting emittance optimization as a function of the number of beam size queries, initialized with 10 random points. To assess the performance of

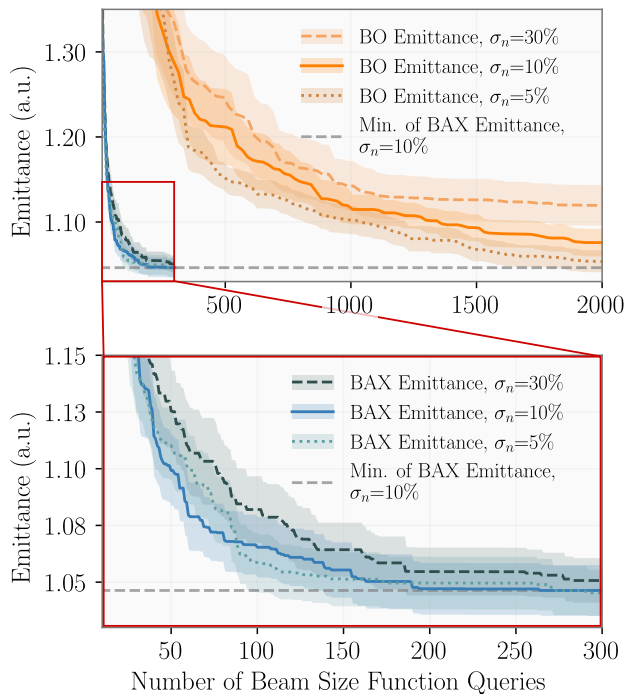


**FIG. 7: Robustness to noise during optimization.** Comparison of the optimization performance on the LCLS injector surrogate model with varying levels of added noise on the beam size for BAX (blue shades) and BO (orange shades). The best emittance up to that iteration is shown, normalized by the minimum of the ground truth emittance. The lower plot shows a magnified view of BAX optimization.

BAX, full experimental emittance scans were performed every 10 iterations at the optimal control variables found by BAX at that iteration (blue). The full emittance scans are slow and are only needed to assess convergence for the study, and would not need to be used in regular accelerator operation. Because an operator would not have access to such scans, it would not be possible to select an earlier setting with better emittance as would be done with BO. Therefore we show an upper bound on emittance at each point (green), i.e. the worst emittance seen after that iteration. Even without full emittance scans, an operator can monitor the improvement in the BAX beam-size prediction compared to the measured values (gray) or the settling of control variables to decide when BAX has converged. BAX reaches a final emittance of  $0.62 \pm 0.02$  mm-mrad, 24% lower than that achieved by accelerator operators via hand-tuning during normal operations with the same machine state ( $0.82 \pm 0.02$  mm-mrad, in red with the shading corresponding to its 2-sigma error). The matching parameter was 1.17 in the X-plane and 1.08 in the Y. We note that neither the matching quadrupoles nor the match were included in this optimization.

We can see that BAX converges to small beam-size errors and a low emittance value after approximately 70 iterations, corresponding to about 20 minutes of beam

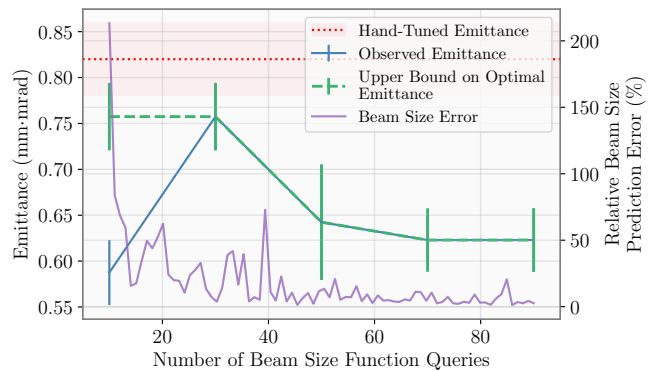


**FIG. 8: Emittance optimization in the LCLS injector.** Results of the BAX emittance optimization showing the true (observed) emittance measured at the optimal configuration identified by BAX every 10 iterations (blue), its upper bound, i.e. the worst emittance seen after that iteration (green), the error on the BAX beam-size prediction compared to the true beam size (purple), and the best hand-tuned emittance on that day for reference (red).

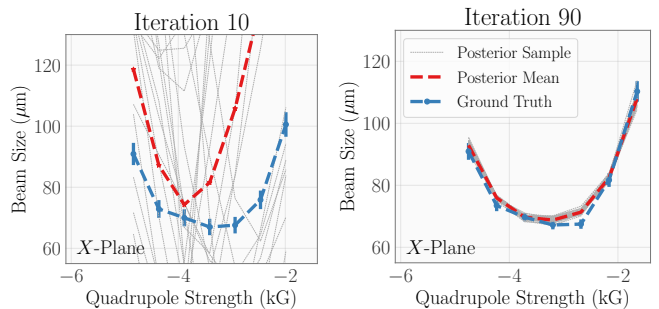


**FIG. 9: BAX beam-size predictions in the LCLS injector.** Comparison of the beam-size predictions in BAX given by the posterior samples of the emittance scan (gray) and the posterior mean of the GP (red) at the estimated optimal configuration, and the true observed beam sizes (blue) for an emittance scan after 10 iterations (left) and 90 iterations (right).

time. We note that BAX happens to select a control setting with low emittance after just 10 queries, however we can see from the internal model error (purple line in Fig. 8) that this occurred by chance. The error on the predictions is still large when the initial low emittance value is encountered at iteration 10, and only reduces to fluctuations within the measurement error after approximately 60 iterations.

We can also confirm that by the end of the optimization, the GP has learned an accurate model of emittance scans in the secondary domain, as seen in Fig. 9. For iterations 10 and 90, we plot the posterior samples of the emittance scan (gray) at the optimal configuration that BAX estimates at that iteration, the posterior mean of

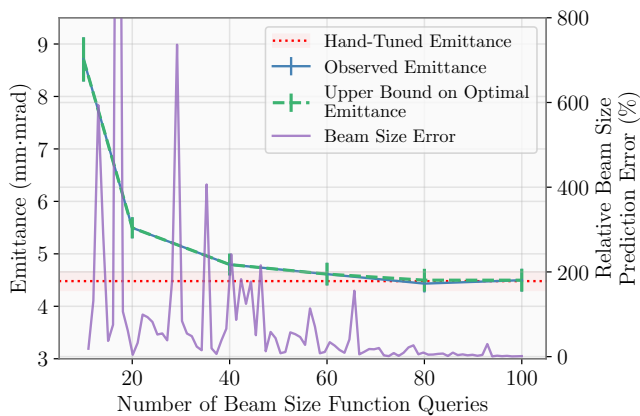


**FIG. 10: Emittance optimization in the FACET-II injector.** Results of the BAX emittance optimization showing the true (observed) emittance measured at the optimal configuration identified by BAX every 10 iterations (blue), its upper bound, i.e. the worst emittance seen after that iteration (green), the error on the BAX beam-size prediction compared to the true beam size (purple), and the best hand-tuned emittance on that day for reference (red).

the GP (red), and the true beam-size measurements for this scan (blue). We can see that at iteration 10, BAX has not yet learned to model emittance scans accurately, again confirming the low emittance in Fig. 8 was selected by chance at that iteration.

The BAX behavior in this experimental setting is consistent with the simulation study on the injector surrogate model. Due to inefficiency of traditional optimizers, the performance could not be compared on the LCLS machine, as a single BO run was expected to take several hours based on previous experience, and beam time at LCLS is in high demand. Nonetheless, these results are a strong indication that BAX performance surpasses standard black-box optimization methods in noisy experimental settings, just as we observed in the simulation environment.

In addition to the experimental test on LCLS, we applied the BAX procedure to the optimization of the electron beam emittance on FACET-II. The FACET-II injector line has an identical setup to the LCLS beam line, and we again optimized SOL1, CQ1 and SQ1. However, FACET-II has a charge of 2 nC, compared to 250 pC in the LCLS test. The control domain bounds were (0.37, 0.41) (kG·m) for SOL1, and (-0.01, 0.01) (kG) for CQ1 and SQ1. Here, optical transition radiation (OTR) screens were used instead of wire scanners for measuring the beam size downstream of the injector (see Methods).

BAX was initialized with 10 random beam-size measurements, and full emittance evaluations were performed every 10 iterations using the current optimal control variables. Figure 10 shows the results of the FACET-II experimental run. Following the 10 initial random

samples, BAX converges to an optimal configuration after 80 queries, recovering a similar emittance ( $4.49 \pm 0.11$  mm-mrad, with a match of 1.07 in  $X$ -plane and 1.06 in  $Y$ ) to the best hand-tuned value found during normal operations that day ( $4.48 \pm 0.09$  mm-mrad, with a match of 1.05 in  $X$  and 1.02 in  $Y$ ). Similarly to previous figures, we also show the error on the BAX beam-size prediction compared to the true beam size measured on the machine at every iteration.

## DISCUSSION

In summary, we have proposed a new approach for highly-efficient optimization of systems involving multi-point measurements, and have implemented the method experimentally for the high-impact case of emittance optimization in accelerators. By building a model in the joint control-measurement domain, BAX can query single points in the measurement domain while sharing that information across different queries, thereby maximizing the information gain of each measurement and increasing the overall efficiency of optimization. We applied BAX to the specific task of electron beam emittance optimization in the LCLS injector in both noisy simulation and experimental settings, and in the FACET-II injector in an experimental setting. In simulation with typical LCLS noise levels, we saw a  $20\times$  increase in efficiency in reaching the optimum when using BAX compared to BO. In experiments on the live machine, BAX was able to reach an emittance that was 24% lower than that achieved by hand-tuning at LCLS, and recovered a similar emittance to the best hand-tuned emittance in FACET-II.

Future work will include expanding the BAX method presented here to higher dimensions to incorporate more quadrupoles and control variables along the accelerator, and targeting more complex objectives (e.g. the beam matching parameter along with the emittance). We expect performance can improve further with stronger priors, such as information on the physical correlations between the control and measurement variables [7]. A variety of other types of queries on accelerators require multi-point measurements and could be used with BAX. In addition to direct optimization, BAX could be used in tandem with more comprehensive machine models, and highlights a new path toward replacing expensive indirect beam measurements with computation on easy-to-acquire samples from surrogate models.

The BAX approach solves a challenging and long-standing tuning problem in accelerators, and we anticipate it to be broadly applicable to complex optimization problems involving multi-point measurements commonly found in science and engineering. While we focus on multi-point measurements, similar advantages exist for single-point queries that produce rich outputs, e.g. running a simulation. BAX is particularly advantageous over traditional methods in high noise environments and with high dimensional inputs, providing a much needed

gain in sample efficiency when optimizing on real-world scientific instruments and devices.

## METHODS

**Experimental Setup.** *LCLS Injector Overview.* The LCLS injector begins with a photocathode RF gun followed by two S-band (2.856 GHz) linac sections (L0a and L0b) producing one or more electron bunches at a 120 Hz repetition rate with an energy of 135 MeV (see Fig. 3) [29]. In this work, the electron bunch charge was 250 pC. The algorithm and analysis software communicated with experimental devices using PyEpics [38], a Python interface to the EPICS Channel Access (CA) library for the EPICS control system.

*LCLS RF Gun and Measurement Quadrupole.* The focusing gun solenoid (SOL1) is located directly downstream of the RF gun and upstream of L0a, and has two small quadrupole coils incorporated into its magnet. These coils, one normal (CQ1) and one skew (SQ1) quadrupole, are single wires spanning the length of the solenoid, and are intended to cancel a small quadrupole field error at the end of SOL1. The measurement (scanning) quadrupole (Q5) is 11.7 m from the gun solenoid, and is separated from the wire scanner by a 2.1-m long drift. Figure 3 shows an illustration of this layout.

*LCLS Beam Diagnostics.* The transverse beam profiles at LCLS were measured with minimally-invasive wire scanners for both  $X$ - and  $Y$ -planes. They require multiple shots for each measurement, and provide a multi-pulse averaged integrated beam profile from photomultiplier tube measurements where a Gaussian distribution was used to extract the RMS beam size from the integrated profiles. The statistical fitting error of 3% on average was propagated to the emittance result. The systematic error from the choice of beam size distribution, not taken into account in the experimental emittance results, was estimated to be around 4%/7% in  $X$ -/ $Y$ -plane. Each beam-size measurement took at least 18 seconds to execute a wire scanner measurement. While OTR screens would be faster than wire scanners, only the slow wire measurements were available at LCLS at the time of this paper.

*FACET-II Setup.* The FACET-II injector produces a single electron bunch at a 120 Hz repetition rate with an energy of 125 MeV. In this setup, the measurement quadrupole is 2.7 m from the measurement screen, separated only by a drift. The beam profiles were measured with an OTR screen. For each measurement at each quadrupole setting, after a 3 second wait-time for the magnet to settle, four images were acquired, background subtracted, then averaged. The  $X$ - and  $Y$ -plane beam profile projections of the final image were fitted with a Gaussian distribution whose width was taken as the beam size. The statistical error from the fit (around 3% on average) was propagated to the emittance result.

**Beam Emittance Measurements.** In this work, we

only consider the transverse emittance in the  $X$ - and  $Y$ -dimensions, which represents the area of the beam in the transverse planes defined by the positions and momenta,  $x$  and  $p_x$  in the horizontal plane, and  $y$  and  $p_y$  in the vertical plane (the  $X$ - and  $Y$ -axes are defined as orthogonal and the  $Z$ -axis as parallel to the path of the beam). All mentions of emittance here refer to the geometric mean of the normalized transverse emittance, unless otherwise noted.

Common methods to measure electron beam size in the transverse planes involve either scanning a wire through the beam or passing the beam through a yttrium aluminum garnet (YAG) or OTR screen [39]. An emittance scan is done using either multiple wires/screens at different positions in the accelerator, or, as we used in this work, a single wire/screen while changing an upstream quadrupole magnet [14, 40]. Here, each full emittance scan was performed using the Q5 quadrupole with adaptive scanning methods as outlined in [34]. For each full emittance scan executed on the machine, four initial points are measured as a rough scan along the full quadrupole range to find the approximate waist location, which can change as the upstream injector configuration is varied. Once the waist is found, a finer scan of seven points is measured around the waist, with redundant points skipped during acquisition. During analysis, any data outside of the convex region are removed from the set based on the inflection points, and points are added as needed to recover a symmetric parabola. The process repeats in each of the  $X$  and  $Y$  dimensions, for a total of 18 beam-size measurements on average.

When accelerator operators tune the LCLS photoinjector by hand, emittance calculations typically involve a scan of at least four measurements over the domain of the scanning quadrupole upstream of the wire. However, in some configurations of the injector, the waist of the beam—a necessary feature to capture—in the transverse  $X$ - and  $Y$ -plane does not occur at the same quadrupole strength, thus requiring two quadrupole scans over two different ranges (or one large range). Moreover, to incorporate the calculation into automated tuning, the calculation must be robust, requiring additional measurements. To achieve robust and accurate measurements, the quadrupole scan range needs to be large enough to fully capture the waist of the beam along both axes, while still being narrow enough to accurately quantify the minimum of the parabolic curve. This range can vary for different machine settings and is typically adjusted by hand until a good scan is achieved.

Here, the number of measurements per scan executed on the machine (18 on average) was empirically chosen. Using fewer beam-size measurements per scan was insufficiently robust during optimization, leading to erroneous emittance calculations. Using additional measurements per scan resulted in a slightly smaller final emittance, but at the cost of even slower convergence. BAX uses 30 measurements on the internal model, because acquisition time is many orders of magnitude faster than querying



the machine.

**BAX Algorithm.** We can describe joint measurement and optimization problems as the task of inferring a computable property  $\mathcal{O}_{\mathcal{A}}$  of a potentially noisy black-box function  $f$  given an algorithm  $\mathcal{A}$ . BAX presents a general framework for inferring computable properties  $\mathcal{O}_{\mathcal{A}}$  within  $\mathcal{T}$  function evaluations, given  $\mathcal{A}$  and a prior distribution on  $f$ ,  $p(f)$ , that captures the initial uncertainty about the true function. In this work,  $p(f)$  is defined by a Gaussian process (GP) with a radial basis function (RBF) kernel, and we denote  $p(f|\mathcal{D}_t)$  as the posterior distribution of  $f$  given a dataset  $\mathcal{D}$  of  $t - 1$  observations. We then use  $p(\mathcal{O}_{\mathcal{A}}|\mathcal{D}_t)$  to denote the induced posterior distribution over the algorithm output  $\mathcal{O}_{\mathcal{A}}$ .

To reduce the number of function evaluations, we use an information-based BAX method, InfoBAX [22, 30, 31], to make targeted queries that maximize the mutual information between  $\mathcal{O}_{\mathcal{A}}$  and the next observation  $y_t$ . The InfoBAX procedure is a sequential algorithm that seeks to maximize the acquisition function, defined here as the expected information gain (EIG) about  $\mathcal{O}_{\mathcal{A}}$  upon observing  $y_t$ . The next sampling point is then chosen to be the  $x_t$  that maximizes the estimated EIG. We can write EIG as

$$\text{EIG}_t(x) = \text{H}[\mathcal{O}_{\mathcal{A}}|\mathcal{D}_t] - \mathbb{E}_{p(y_x|\mathcal{D}_t)}[\text{H}[\mathcal{O}_{\mathcal{A}}|\mathcal{D}_t \cup \{(x, y_x)\}]],$$

where  $\text{H}[\mathcal{O}_{\mathcal{A}}|\mathcal{D}_t]$  is the entropy of  $p(\mathcal{O}_{\mathcal{A}}|\mathcal{D}_t)$ , and  $p(y_x|\mathcal{D}_t)$  is the posterior predictive distribution at  $x$  given  $\mathcal{D}_t$ . For details on how  $\text{EIG}(x)$  is estimated, we refer the reader to [22].

To compute EIG efficiently, the InfoBAX procedure only executes the algorithm  $\mathcal{A}$  on function samples  $\tilde{f}$  drawn from the posterior distribution  $p(f|\mathcal{D}_t)$ , similar to other posterior sampling-based methods for experimental design [41, 42]. In this manner, the true algorithm output is inferred with minimal evaluations of the true function  $f$  (e.g. emittance as a function of accelerator tuning settings). Once the next sampling point is selected at each iteration, a single evaluation of the true function is made at that selected point.

**BAX Computational Considerations.** One potential hurdle for the implementation of the BAX algorithm is the computational complexity, as each iteration requires repeated application of the algorithm  $\mathcal{A}$  on draws from the model posterior, which can require a large number of emittance calculations. Although this work did not focus on computational efficiency of the algorithm, in cases where  $\mathcal{A}$  is expensive, parallelization of the BAX algorithm execution procedure can significantly reduce wall-clock time. In the case of emittance optimization at LCLS, a parallelized version using five CPU cores takes 4.7 seconds, on average, to select a beam-size function query at each iteration of the algorithm.

**LCLS Injector Surrogate Model.** The LCLS injector surrogate model used in this work is a neural network (NN) based surrogate model that provides fast, non-invasive predictions of electron beam properties. The NN was trained on IMPACT-T simulation [43] data us-

ing 16 input parameters including the pulse length, laser radius, gun solenoid and quadrupole settings, L0 linac phase, and all matching quadrupoles settings. The NN architecture consists of 17 layers, and the model outputs scalar predictions of the  $X$ - and  $Y$ -plane beam sizes. To mimic experimental emittance measurement procedures in a simulation setting, the  $X$ -,  $Y$ -plane beam sizes were used when performing a beam size query, and Gaussian noise  $\mathcal{N}(0, \sigma_n)$  was added to each beam size before passing the measurements to the emittance calculation.

**Algorithm Comparison in Simulation Setting.** Bayesian optimization was implemented using the **Bayesian Optimization** package [44]. We defined the BO’s surrogate model as a GP constructed with an RBF kernel, and the upper confidence bound (UCB) as the acquisition function with an exploration weight of 2.0 which was maximized to select the next function query. For each run, BO was initialized with three random scans that were uniformly and randomly sampled from the control domain. The simplex algorithm was implemented using the optimization routine available through SciPy [45]. Each simplex optimization was run with an initial guess of the injector configuration that was randomly sampled from the control domain as well.

In some cases when using the NN and querying points far from optimal, the emittance calculation fails to return a number. Such cases were handled by assigning a large number to simplex queries, and the BAX and BO algorithms were set to pass any failed measurements and move to the next optimal point in the acquisition function optimization. Additionally, any emittance measurements with an uncertainty larger than 70% were ignored by the BO and BAX optimizers.

## ACKNOWLEDGEMENTS

We would like to thank Nicole Neveu for her help in setting up the LCLS emittance measurements, Finn O’Shea for his feedback on the emittance measurement procedures, and Feng Zhou and John Sheppard for their guidance and support with the LCLS injector machine development time.

## AUTHOR CONTRIBUTIONS

A.E. and D.R. conceived of adapting BAX to emittance optimization; S.A.M., W.N. and A.E. ran the experiments; S.A.M. and W.N. wrote the software; W.N. developed the BAX algorithm; S.A.M. performed the surrogate model optimizations; A.E. and C.M. contributed to the software; C.E., W.C. and T.M. J.G. contributed to the experimental runs; S.E., A.E., and D.R. provided guidance and oversight; S.A.M., W.N., A.E., and D.R. wrote the manuscript with input from all co-authors.

## COMPETING INTERESTS

The authors declare no competing interests.

## REFERENCES

- [1] Jones, D. R., Schonlau, M. & Welch, W. J. Efficient global optimization of expensive black-box functions. *Journal of Global optimization* **13**, 455–492 (1998).
- [2] Brochu, E., Cora, V. M. & de Freitas, N. A tutorial on bayesian optimization of expensive cost functions, with application to active user modeling and hierarchical reinforcement learning. *CoRR abs/1012.2599* (2010). URL <http://arxiv.org/abs/1012.2599>. 1012.2599.
- [3] Kushner, H. J. A new method of locating the maximum point of an arbitrary multipeak curve in the presence of noise. In *Joint Automatic Control Conference*, 1, 69–79 (1963).
- [4] Moćkus, J. On bayesian methods for seeking the extremum. In Marchuk, G. I. (ed.) *Optimization Techniques IFIP Technical Conference Novosibirsk, July 1–7, 1974*, 400–404 (Springer Berlin Heidelberg, Berlin, Heidelberg, 1975).
- [5] McIntire, M., Cope, T., Ermon, S. & Ratner, D. Bayesian Optimization of FEL Performance at LCLS. In *7th International Particle Accelerator Conference*, WEPOW055 (2016).
- [6] Kirschner, J., Mutný, M., Hiller, N., Ischebeck, R. & Krause, A. Adaptive and safe bayesian optimization in high dimensions via one-dimensional subspaces (2019). URL <https://arxiv.org/abs/1902.03229>.
- [7] Duris, J. *et al.* Bayesian optimization of a free-electron laser. *Phys. Rev. Lett.* **124**, 124801 (2020). URL <https://link.aps.org/doi/10.1103/PhysRevLett.124.124801>.
- [8] Shaloo, R. J. *et al.* Automation and control of laser wakefield accelerators using bayesian optimization. *Nature Communications* **11** (2020). URL <https://doi.org/10.1038/s41467-020-20245-6>.
- [9] Roussel, R., Hanuka, A. & Edelen, A. Multiobjective bayesian optimization for online accelerator tuning. *Physical Review Accelerators and Beams* **24** (2021). URL <https://doi.org/10.1103/PhysRevAccelBeams.24.062801>.
- [10] Terayama, K., Iwata, H., Araki, M., Okuno, Y. & Tsuda, K. Machine learning accelerates MD-based binding pose prediction between ligands and proteins. *Bioinformatics* **34**, 770–778 (2017). URL <https://doi.org/10.1093/bioinformatics/btx638>. <https://academic.oup.com/bioinformatics/article-pdf/34/5/770/25117719/btx638.pdf>.
- [11] Yamashita, T. *et al.* Crystal structure prediction accelerated by bayesian optimization. *Phys. Rev. Materials* **2**, 013803 (2018). URL <https://link.aps.org/doi/10.1103/PhysRevMaterials.2.013803>.
- [12] Miskovich, S. A. *et al.* Online bayesian optimization for a recoil mass separator. *Phys. Rev. Accel. Beams* **25**, 044601 (2022). URL <https://link.aps.org/doi/10.1103/PhysRevAccelBeams.25.044601>.
- [13] Lauber, S. *et al.* Longitudinal phase space reconstruction for a heavy ion accelerator. *Phys. Rev. Accel. Beams* **23**, 114201 (2020). URL <https://link.aps.org/doi/10.1103/PhysRevAccelBeams.23.114201>.
- [14] Minty, M. & Zimmermann, F. *Measurement and Control of Charged Particle Beams* (Springer Berlin Heidelberg, 2003).
- [15] Emma, P. *et al.* First lasing and operation of an ångstrom-wavelength free-electron laser. *Nature Photonics* **4**, 641–647 (2010). URL <https://doi.org/10.1038/nphoton.2010.176>.
- [16] Huang, Z. & Kim, K.-J. Review of x-ray free-electron laser theory. *Phys. Rev. ST Accel. Beams* **10**, 034801 (2007). URL <https://link.aps.org/doi/10.1103/PhysRevSTAB.10.034801>.
- [17] Schoenlein, R. W. Lcls-ii high energy (lcls-ii-he): A transformative x-ray laser for science (2016). URL <https://www.osti.gov/biblio/1634206>.
- [18] Brinkmann, R., Derbenev, Y. & Flöttmann, K. A low emittance, flat-beam electron source for linear colliders. *Phys. Rev. ST Accel. Beams* **4**, 053501 (2001). URL <https://link.aps.org/doi/10.1103/PhysRevSTAB.4.053501>.
- [19] Benedikt, M., Schulte, D. & Zimmermann, F. Optimizing integrated luminosity of future hadron colliders. *Phys. Rev. ST Accel. Beams* **18**, 101002 (2015). URL <https://link.aps.org/doi/10.1103/PhysRevSTAB.18.101002>.
- [20] Piot, P., Sun, Y.-E. & Kim, K.-J. Photoinjector generation of a flat electron beam with transverse emittance ratio of 100. *Phys. Rev. ST Accel. Beams* **9**, 031001 (2006). URL <https://link.aps.org/doi/10.1103/PhysRevSTAB.9.031001>.
- [21] Ody, A. *et al.* Flat electron beam sources for dfa accelerators. *Nuclear Instruments and Methods in Physics Research Section A: Accelerators, Spectrometers, Detectors and Associated Equipment* **865**, 75–83 (2017). URL <https://www.sciencedirect.com/science/article/pii/S0168900216310877>. Physics and Applications of High Brightness Beams 2016.
- [22] Neiswanger, W., Wang, K. A. & Ermon, S. Bayesian algorithm execution: Estimating computable properties of black-box functions using mutual information. In *International Conference on Machine Learning* (PMLR, 2021).
- [23] Nelder, J. A. & Mead, R. A Simplex Method for Function Minimization. *The Computer Journal* **7**, 308–313 (1965). URL <https://doi.org/10.1093/comjnl/7.4.308>. <https://academic.oup.com/comjnl/article-pdf/7/4/308/1013182/7-4-308.pdf>.
- [24] Yakimenko, V. *et al.* Facet-ii facility for advanced accelerator experimental tests. *Phys. Rev. Accel. Beams* **22**, 101301 (2019). URL <https://link.aps.org/doi/10.1103/PhysRevAccelBeams.22.101301>.
- [25] Wang, J., Wang, D. & Reiser, M. Beam emittance measurement by the pepper-pot method. *Nuclear Instruments and Methods in Physics Research Section A: Accelerators, Spectrometers, Detectors and Associated Equipment* **307**, 190–194 (1991). URL <https://www.sciencedirect.com/science/article/pii/016890029190182P>.
- [26] Thangaraj, J. C. T. & Piot, P. A high-resolution multi-slit phase space measurement technique for low-emittance beams. In Zgadzaj, R., Gaul, E. & Downer, M. C. (eds.) *Advanced Accelerator Concepts: 15th Advanced Accelerator Concepts Workshop*, vol. 1507 of *American Institute of Physics Conference Series*, 757–

- 761 (2012).
- [27] Zhang, M. Emittance formula for slits and pepper pot measurement (1996).
- [28] Strehl, P. *Measurements in Phase Spaces*, 213–283 (Springer Berlin Heidelberg, Berlin, Heidelberg, 2006). URL [https://doi.org/10.1007/3-540-26404-3\\_6](https://doi.org/10.1007/3-540-26404-3_6).
- [29] Akre, R. *et al.* Commissioning the linac coherent light source injector. *Phys. Rev. ST Accel. Beams* **11**, 030703 (2008). URL <https://link.aps.org/doi/10.1103/PhysRevSTAB.11.030703>.
- [30] Moosbauer, J., Casalichio, G., Lindauer, M. & Bischl, B. Enhancing explainability of hyperparameter optimization via bayesian algorithm execution. *arXiv preprint arXiv:2206.05447* (2022).
- [31] Mehta, V., Paria, B., Schneider, J., Ermon, S. & Neiswanger, W. An experimental design perspective on model-based reinforcement learning. In *International Conference on Learning Representations* (2021).
- [32] Chaloner, K. & Verdinelli, I. Bayesian experimental design: A review. *Statistical Science* 273–304 (1995).
- [33] Settles, B. Active learning. *Synthesis lectures on artificial intelligence and machine learning* **6**, 1–114 (2012).
- [34] Miskovich, S. A., Edelen, A. & Mayes, C. PyEmitance: A general python package for particle beam emittance measurements with adaptive quadrupole scans. In *The 13th International Particle Accelerator Conference*. IPAC22 (JACoW Publishing, Geneva, Switzerland, 2022).
- [35] Tomin, S. *et al.* Progress in Automatic Software-based Optimization of Accelerator Performance. In *7th International Particle Accelerator Conference*, WEPOY036 (2016).
- [36] Hanuka, A. *et al.* Online tuning and light source control using a physics-informed gaussian process adi (2019). URL <https://arxiv.org/abs/1911.01538>.
- [37] Roussel, R. *et al.* Turn-key constrained parameter space exploration for particle accelerators using bayesian active learning. *Nature Communications* **12**, 5612 (2021).
- [38] Newville, M. *et al.* pyepics/pyepics 3.4.0 (2019). URL <https://zenodo.org/record/3241645>.
- [39] Loos, H. *et al.* Operational performance of lcls beam instrumentation (2010). URL <https://www.osti.gov/biblio/982082>.
- [40] Loehl, F. Measurements of the transverse emittance at the VUV-FEL. Tech. Rep. 1435-8085, Germany (2005).
- [41] Hernández-Lobato, J. M., Hoffman, M. W. & Ghahramani, Z. Predictive entropy search for efficient global optimization of black-box functions. *Advances in neural information processing systems* **27** (2014).
- [42] Kandasamy, K. *et al.* Myopic posterior sampling for adaptive goal oriented design of experiments. In *International Conference on Machine Learning*, 3222–3232 (PMLR, 2019).
- [43] Qiang, J., Lidia, S., Ryne, R. D. & Limborg-Deprey, C. Three-dimensional quasistatic model for high brightness beam dynamics simulation. *Phys. Rev. ST Accel. Beams* **9**, 044204 (2006). URL <https://link.aps.org/doi/10.1103/PhysRevSTAB.9.044204>.
- [44] Nogueira, F. Bayesian Optimization: Open source constrained global optimization tool for Python (version 1.1) (2014). URL <https://github.com/fmfn/BayesianOptimization>.
- [45] Virtanen, P. *et al.* SciPy 1.0: Fundamental Algorithms for Scientific Computing in Python, (version 1.7.3). *Nature Methods* **17**, 261–272 (2020).